International Journal of Offshore and Polar Engineering (ISSN 1053-5381)

Vol. 33, No. 4, December 2023, pp. 399–408; https://doi.org/10.17736/ijope.2023.ak58

http://www.isope.org/publications

Numerical Study of Green Water Loads on a Fixed Structure with Various Gate Release Velocities by the MPS Method

Mengmeng Wu*, Weiwen Zhao* and Decheng Wan*†
Computational Marine Hydrodynamics Lab, School of Naval Architecture, Ocean and Civil Engineering
Shanghai Jiao Tong University, Shanghai, China

Jifei Wang
Shanghai Aerospace System Engineering Institute
Shanghai, China

In rough sea conditions, a large mass of water will exceed the freeboard and cause violent slamming on the deck, which is known as green water. Many scholars have devoted themselves to the study of green water because of its strong destructiveness. Upon considering the complexity of green water, different simplified methods have been used to study its mechanism and loads. This paper investigates green water loads and patterns on a fixed structure using the meshless particle solver MLParticle-SJTU, which is based on the moving particle semi-implicit (MPS) method. A serial rapid flow-structure interaction was generated by the wet dam-break method. The experimental study by Hernández-Fontes et al. in 2020 investigated vertical loads of green water, and the numerical work by Areu-Rangel et al. in 2021 continued to study horizontal loads. In this paper, the study was extended by analyzing the effects of different gate release velocities on the generated wave patterns and green water loads. The results obtained in this paper were in good agreement with the existing results. Moreover, the influence of different gate release speeds on the green water simulation was analyzed.

INTRODUCTION

Marine structures are vulnerable to wave intrusion. In harsh seas, these incoming waves are likely to exceed the freeboard, break over the deck, and flow onto the deck. This phenomenon is known as green water or water shipping (Greco et al., 2004). Green water in rough seas will cause adverse effects such as damage to superstructures and hull structures, accidental overloading of ships, injuries to personnel, and damage to equipment, to name a few. Therefore, it is of great practical importance to study the physical mechanism of the green water events, to predict the wave on the deck, and to assess its impact on the safety and performance of ships and offshore platforms.

The green water phenomenon has been studied using experimental (Fonseca and Soares, 2005), theoretical (Zhang et al., 1996), and numerical tools. The current research mainly focuses on the identification of the types of water shipping events (e.g., the dam-breaking type, plunging-wave type, and hammer-fist type) as described by Greco et al. (2007), the evolution process of the water on the deck (Le Touzé et al., 2010), the wave loads (Nielsen and Mayer, 2004), and so on. With the rapid development of computer technology, computational fluid dynamics (CFD) techniques based on the meshless method and the mesh-based method (Silva et al., 2017; Rosetti et al., 2019) have been used to study the green water phenomena. Grid generation in mesh methods needs heavy efforts. Meshless methods are expected to solve the troubles concerning the grid. The particle method, which discretizes the computational domain in a set of particles, is one of the widely used meshless methods. In the mesh method, when dealing with problems such as wave surface rolling, crushing, and splashing, it is necessary to introduce special free surface treatment methods. However, the particle method can track free surfaces with arbitrarily large deformations without the need for additional interface capture and reconstruction algorithms, in contrast with the mesh-based method. Scholars have conducted a lot of studies based on the particle method because of its natural advantages in simulating large deformations of the free surface (Luo et al., 2021)—for example, the dam-break flow (Tang, Zhang and Wan, 2016; Chen and Wan, 2019), water entry problems (Tang, Wan, et al., 2016), wave-ship interactions (Shibata et al., 2012), liquid sloshing problems (Zhang et al., 2014, 2021; Khayyer et al., 2023), multiphase flows (Shimizu et al., 2020; Wen et al., 2021b), fluid-structure interactions (Khayyer et al., 2017; Zhang et al., 2019), and so on.

A number of scholars have applied particle methods to study the phenomenon of green water. The effect of a green water event on a structure depends on certain factors such as the geometry and motion conditions of the structure and the characteristics of the incident wave. In the numerical simulation of green water events using particle methods, regular waves, solitary waves, and other methods were often used to reproduce the harsh sea conditions. Shibata and Koshizuka (2007) simulated the water shipping phenomenon on the bow deck of a three-dimensional fixed ship under the action of solitary waves, using the moving particle semi-implicit (MPS) method for the prediction of the impact pressure on the deck. Good agreement was obtained with the experiment in terms of wave pattern, wave height, and impact pressure on the deck. Kawamura et al. (2016) applied the smoothed particle hydrodynamics (SPH) method to predict the motion of a fishing vessel under green water conditions generated by steep regular waves, and this SPH simulation well presented the green water events and wave reflection. On the basis of the MPS method, Zhang et al. (2016) studied the green water phenomenon of solitary waves hitting a plate structure and analyzed the trend of

*ISOPE Member; †Corresponding author.
Received August 16, 2023; updated and further revised manuscript received by the editors September 19, 2023. The original version (prior to the final updated and revised manuscript) was presented at the Thirty-third International Ocean and Polar Engineering Conference (ISOPE-2023), Ottawa, Canada, June 18–23, 2023.
KEY WORDS: Green water, moving particle semi-implicit (MPS), wave loads, wet dam-break method, gate release velocity.

impact loads on the plate and the wave evolution process under the interaction between solitary waves and structures.

Green water events are complex phenomena that occur rapidly. To investigate the features and loads generated by isolated green water events, a systematic alternative wet dam-break method has been used to generate the incident wave in recent studies. The wet dam-break method is similar to the dam-break phenomenon. The wet dam-break can be regarded as adding a certain height of water downstream of the dam break. Khayyer and Gotoh (2010) simulated the wave generated by wet dam-break method using standard and improved versions of three particle methods—namely, the MPS, the incompressible smoothed particle hydrodynamics, and the weakly compressible smoothed particle hydrodynamics method—and compared results with experiments. The work highlighted the potential capabilities of particle methods in reproducing detailed features of a wet dam break. The dam-break waves flowing over dry and wet beds were investigated experimentally and numerically by Garoosi et al. (2022). It was found that although both MPS and volume-of-fluid (VOF) models could capture morphological changes of dam-break flows, the MPS, in general, outperformed the VOF in handling nonlinear multiphase phenomena involving wave breaking and splashing. This verified the accuracy of the MPS method in the wet dam-break simulation.

The experimental study by Hernández-Fontes et al. (2020) investigated the vertical loads on a fixed structure in the case of water shipping, and the numerical work by Areu-Rangel et al. (2021) further investigated horizontal loads. In these studies, the green water events were generated by the wet dam-break method. The wet dam-break method is very friendly to both experiments and numerical simulations in analyzing different green water events because it is simple and can produce systematic, repeatable, and short-duration green water events. To realize the condition of the wet dam-break method in an experiment, a gate was used to control the water at the beginning of the experiment. It can be seen that the incident waves of the experiment of Hernández-Fontes et al. (2020) with a gate and the numerical simulation of Areu-Rangel et al. (2021) without a gate produced different incident wave patterns. This shows that the gate had a certain influence on the wave formation and the green water events generated. This paper seeks to analyze the differences among the green water events generated by the wet dam-break method caused by different gate release speeds using the same model as Areu-Rangel et al. (2021).

The effect of different gate speeds on the waveform formed by the dam-break method based on experiments and SPH simulations was investigated by von Häfen et al. (2019). The motion of the gate resulted in a difference associated with the propagation of the wave. The slower the gate opening, the greater the difference. The difference was particularly pronounced in the near field and decreased with increasing distance from the gate. Ye and Zhao (2017) used a two-liquid VOF-based model to investigate the influence of gate removal acceleration on the early stages of wet dam-break flow. The gate release acceleration affected the evolution of the free surface and water-water interface profiles. With an increase in gate acceleration, the formation and evolution of jet flow and dam-break wave would happen earlier. Unfortunately, only three gate removal accelerations were used in the numerical simulation. Apart from this, few experiments as well as numerical simulations have been carried out to investigate the effect of gate release speeds in the wet dam-break method.

To better analyze the effects of the gate release speeds in wave patterns and loads of green water events generated in the model used by Areu-Rangel et al. (2021) and Hernández-Fontes et al. (2020), this paper used the meshless particle solver MLParticle-SJTU based on the MPS method to simulate the water shipping events under different gate release speeds.

NUMERICAL METHOD

The MPS method is a meshless particle method and discretizes the fluid and solid parts in a set of particles endowed with physical characteristics such as mass, velocity, acceleration, and so on (Koshizuka and Oka, 1996). These particles interact through the kernel function. As the distance between particles becomes smaller, the interaction between them becomes greater. The fluid is controlled by the governing equation based on the Lagrangian method.

Governing Equation

The governing equations include the continuity equation and the momentum equation. The governing equation for viscous incompressible flow can be written as

$$\frac{1}{\rho}\frac{D\rho}{Dt} = -\nabla \cdot \boldsymbol{V} = 0 \tag{1}$$

$$\frac{D\boldsymbol{V}}{Dt} = -\frac{1}{\rho}\nabla P + \nu \ \nabla^2 \boldsymbol{V} + \boldsymbol{g} \tag{2}$$

where ρ is the fluid density, $\boldsymbol{V}$ is the velocity vector, P represents the pressure, ν is the kinematic viscosity, $\boldsymbol{g}$ is the gravitational acceleration vector, and t indicates the time. In this paper, the fluid density ρ is 10^3 kg/m^3, and the kinematic viscosity ν is 1.01×10^{-6} m^2/s.

Numerical Models

Kernel Function. In the MPS method, the interaction between particles is realized by the kernel function (Koshizuka and Oka, 1996; Ataie-Ashtiani and Farhadi, 2006). The kernel function of the improved MPS method (Zhang et al., 2014) is shown as follows:

$$W(r) = \begin{cases} \dfrac{r_e}{0.85r + 0.15r_e} - 1 & 0 \le r < r_e \\ 0 & r_e \le r \end{cases} \tag{1}$$

where $r = |\boldsymbol{r}_j - \boldsymbol{r}_i|$represents the spacing between particles i and j, and $r_e$is the influence radius. Generally speaking, the influence radius for particle number density and the gradient model is $r_e = 2.1dp$ and is $r_e = 4.1dp$ for the Laplacian model in this paper, where dp is the initial particle space.

Density of the Particle Number. The particle number density is the sum of all particle kernel functions within the radius of influence. It is defined as follows.

$$\langle n \rangle_i = \sum_{j \ne i} W(|\boldsymbol{r}_j - \boldsymbol{r}_i|) \tag{2}$$

For an incompressible fluid, the particle number density is constant.

Gradient Model. The gradient model is used to discretize the pressure gradient in the governing equation. The expression is

$$\langle \nabla P \rangle_i = \frac{D}{n^0} \sum_{j \ne i} \frac{P_j + P_i}{|\boldsymbol{r}_j - \boldsymbol{r}_i|^2} (\boldsymbol{r}_j - \boldsymbol{r}_i) W(|\boldsymbol{r}_j - \boldsymbol{r}_i|) \tag{3}$$

where D represents the dimension, and n^0 represents the initial particle number density.

Divergence Model. Similar to the gradient model, the divergence model is used to discretize the velocity divergence in the governing equation. The expression is as follows.

$$\langle \nabla \cdot \boldsymbol{V} \rangle_i = \frac{D}{n^0} \sum_{j \neq i} \frac{(\boldsymbol{V}_j - \boldsymbol{V}_i) \cdot (\boldsymbol{r}_j - \boldsymbol{r}_i)}{|\boldsymbol{r}_j - \boldsymbol{r}_i|^2} W(|\boldsymbol{r}_j - \boldsymbol{r}_i|) \tag{4}$$

Laplacian Model. The Laplacian model is used to discretize the second derivative in the governing equation, which can be expressed as

$$\langle \nabla^2 \phi \rangle_i = \frac{2D}{n^0 \lambda} \sum_{j \neq i} (\phi_j - \phi_i) W(|\boldsymbol{r}_j - \boldsymbol{r}_i|) \tag{5}$$

where ϕ is an arbitrary scalar function; λ represents the correction of the error introduced by the kernel function, and it can be written as follows.

$$\lambda = \frac{\sum_{j \neq i} W(|\boldsymbol{r}_j - \boldsymbol{r}_i|) |\boldsymbol{r}_j - \boldsymbol{r}_i|^2}{\sum_{j \neq i} W(|\boldsymbol{r}_j - \boldsymbol{r}_i|)} \tag{6}$$

Pressure Poisson Equation

In the MPS method, the pressure Poisson equation (PPE) is used to solve the particle pressure (Khayyer and Gotoh, 2011). The incompressibility of fluid is determined by a divergence-free condition and constant particle number density condition. The Poisson equation adopted in this paper is as follows.

$$\langle \nabla^2 P^{k+1} \rangle_i = (1 - \gamma) \frac{\rho}{\Delta t} \nabla \cdot \boldsymbol{V}_i^* - \gamma \frac{\rho}{\Delta t^2} \frac{\langle n^k \rangle_i - n^0}{n^0} \tag{7}$$

Superscripts k and $k+1$ represent the k and $k+1$ time steps, respectively. γ is a variable parameter representing the proportion of particle number density in the source term of the Poisson equation. In the numerical simulation in this paper, γ takes the value of 0.01 (Tanaka and Masunaga, 2010). $\boldsymbol{V}_i^*$ is the temporary velocity vector, and the superscript asterisk stands for the temporary value, which will be introduced below.

Time Integration

The procedure of the MPS method is divided into two substeps for every time step. First, all terms except the pressure term in the momentum conservation equation are evaluated explicitly, and the temporal velocity vectors and position vectors of particles are computed as follows.

$$\boldsymbol{V}_i^* = \boldsymbol{V}_i^k + \Delta t (\nu \nabla^2 \boldsymbol{V}_i^k + \boldsymbol{g}) \tag{8}$$

$$\boldsymbol{r}_i^* = \boldsymbol{V}_i^* \Delta t + \boldsymbol{r}_i^k \tag{9}$$

Second, the pressure term is solved implicitly according to the pressure Poisson equation by the bi-conjugate gradients stabilized method. Then, the velocity vectors and position vectors of particles are modified as follows.

$$\boldsymbol{V}_i^{k+1} = \boldsymbol{V}_i^* - \frac{\Delta t}{\rho} \nabla P^{k+1} \tag{10}$$

$$\boldsymbol{r}_i^{k+1} = \boldsymbol{V}_i^{k+1} \Delta t + \boldsymbol{r}_i^k \tag{11}$$

Boundary Conditions

Detection of Free Surface Particles. Once a fluid particle is judged to be located on the free surface, its pressure will be forced to be 0, and this will be used as the boundary condition for solving the pressure Poisson equation. In consequence, it is important to determine whether a particle is located on the free surface. The number density of particles can be used to determine whether a particle is on a free surface in the MPS method. When $\langle n \rangle_i < 0.8 n^0$, the particle is considered to be on a free surface. When $\langle n \rangle_i > 0.97 n^0$, the particles are thought to be inside the fluid. For particles with a particle number density between 0.8 and 0.97, it is difficult to distinguish whether the particle is a free surface particle or internal particle. In this paper, the vector function $\boldsymbol{F}$ presented by Zhang et al. (2014) is introduced, as follows:

$$\langle \boldsymbol{F} \rangle_i = \frac{D}{n^0} \sum_{j \neq i} \frac{\boldsymbol{r}_i - \boldsymbol{r}_j}{|\boldsymbol{r}_i - \boldsymbol{r}_j|} W(|\boldsymbol{r}_i - \boldsymbol{r}_j|) \tag{12}$$

where $\boldsymbol{F}$ is a vector that represents the asymmetry distribution of neighboring particles. When $|\langle \boldsymbol{F} \rangle_i| > 0.9 |\boldsymbol{F}|^0$, the particle is considered to be on the free surface. $|\boldsymbol{F}|^0$ stands for $|\boldsymbol{F}|$ at the initial time of the free surface particle.

Solid Boundary Condition. In this paper, the solid boundary is represented by a layer of wall particles and two layers of ghost particles. The calculation of the pressure on the wall particles is the same as that of the fluid particles, solved by the PPE, whereas the pressures of the ghost particles are obtained by interpolation between the one layer of wall particles and the fluid particles. The advantage of this arrangement is that it can ensure a smooth and accurate pressure field around the solid surface and prevent fluid particles from penetrating into the impermeable boundary. The no-slip boundary condition of Wen et al. (2021a) is used in this paper. To impose the no-slip boundary condition, mirror particles are introduced to replace the wall and ghost particles in the viscous force calculation. The positions of the mirror particles are symmetrical to the corresponding fluid particles around the wall, and the velocities of the mirror particles are calculated using the following equations:

$$\boldsymbol{V}_{mirror} \cdot \boldsymbol{t} = (2\boldsymbol{V}_w - \boldsymbol{V}_f) \cdot \boldsymbol{t} \tag{13}$$

$$\boldsymbol{V}_{mirror} \cdot \boldsymbol{n} = (2\boldsymbol{V}_w - \boldsymbol{V}_f) \cdot \boldsymbol{n} \tag{14}$$

where $\boldsymbol{n}$ and $\boldsymbol{t}$ are the normal and tangential vectors of the wall, respectively. The subscripts *mirror*, w, and f represent the mirror, the wall, and the corresponding fluid particles, respectively.

NUMERICAL SIMULATIONS

Validation of MPS Method

First, the accuracy of the MPS method and the solver MLParticle-SJTU was verified by the above-mentioned SPH simulation using DualSPHysics software (Areu-Rangel et al., 2021). The SPH simulation of Areu-Rangel et al. used the wet dam-break method to generate the incident wave, and a fixed rectangular structure was placed on the right side of the tank, which can be seen as a simplified bow or other structure. The wall on the right-hand side of the tank can be considered to be the side wall of the superstructure on the fixed structure.

The simulation model of Areu-Rangel et al. is shown in Fig. 1. Three wave probes—WP0, WP1, and WP2—have been arranged. A 0.18 m long force measurement element was placed on the top

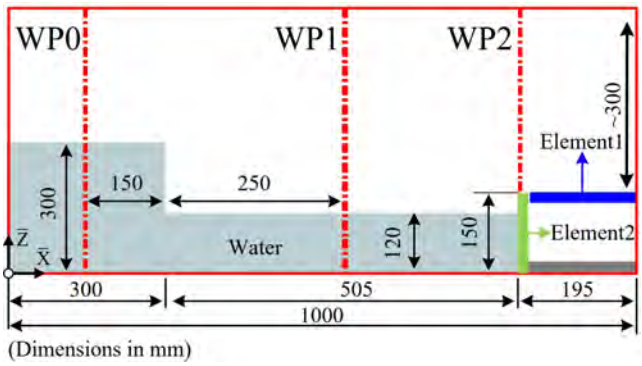

Fig. 1 The sketch of the water shipping model studied by Areu-Rangel et al. (2021), indicating the positions of the three wave probes and two structural elements for the investigation of the hydrodynamic loads

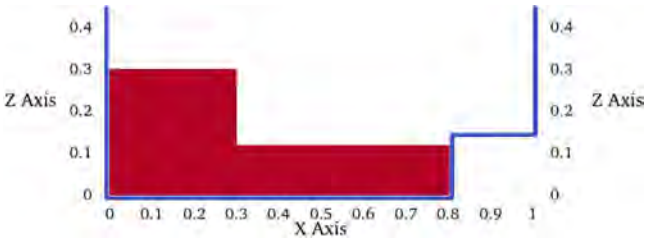

Fig. 2 The sketch of the model used in validation of MPS simulation

of the right-hand fixed structure, and a 0.15 m high force measurement element was placed on the left-hand side of the structure. These arrangements were used to measure water elevations of the incident wave (WP0 and WP1, as shown in Fig. 1), freeboard exceedance (WP2), vertical loads on the deck (Element1), and the horizontal loads of left side of structure (Element2). The other specific dimensions are also shown in Fig. 1.

To reduce the total number of particles and save computational resources, the simplified model shown in Fig. 2 was used in the MPS simulation in this paper, which can achieve the same simulation objective as in Areu-Rangel et al. In line with the SPH simulation, the start time of the water movement in the MPS simulation was also set to 0.5 s. The simulation time interval was set to 0.0002 s, whereas the time-step algorithm was the Verlet algorithm, and the initial particle spacing was 0.0005 m in the simulation of Areu-Rangel et al.

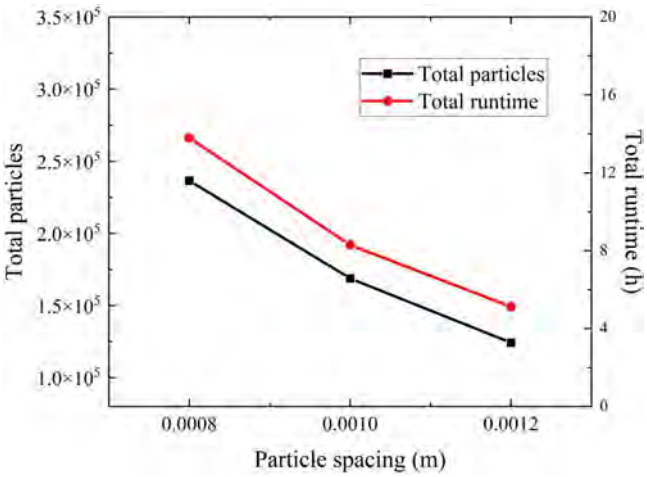

Fig. 3 The information about particle spacing sensitivity analysis: Total particles and total runtime

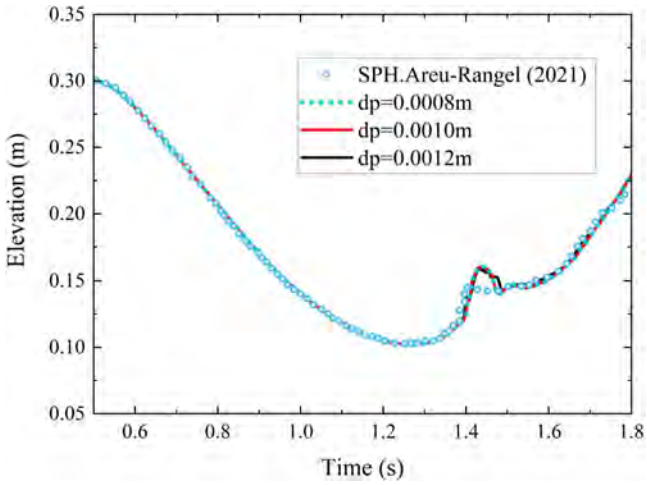

(a) WP0

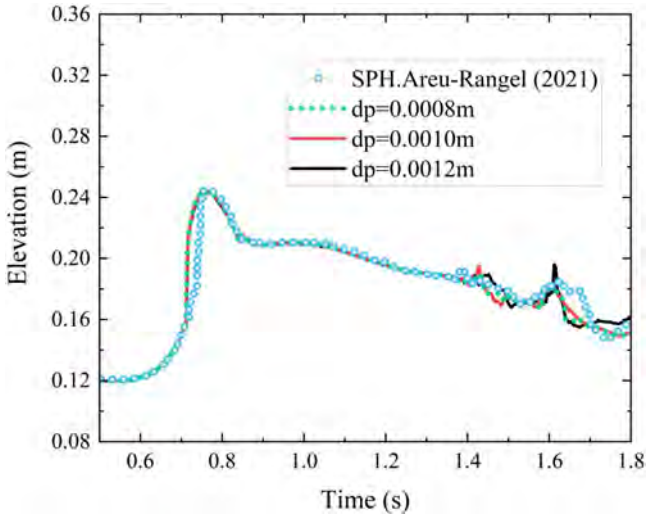

(b) WP1

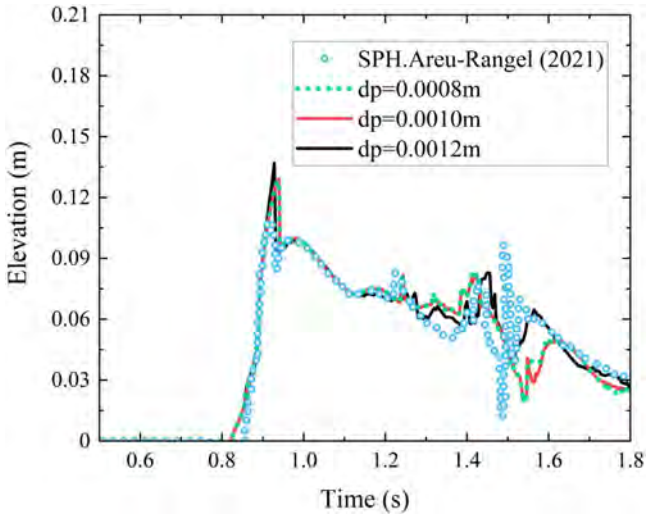

(c) WP2

Fig. 4 Validation of the numerical approach: Comparison of the wave elevations between the SPH results and MPS results with three different particle spacings: (a) Water elevations at WP0, (b) water elevations at WP1, and (c) water elevations at WP2

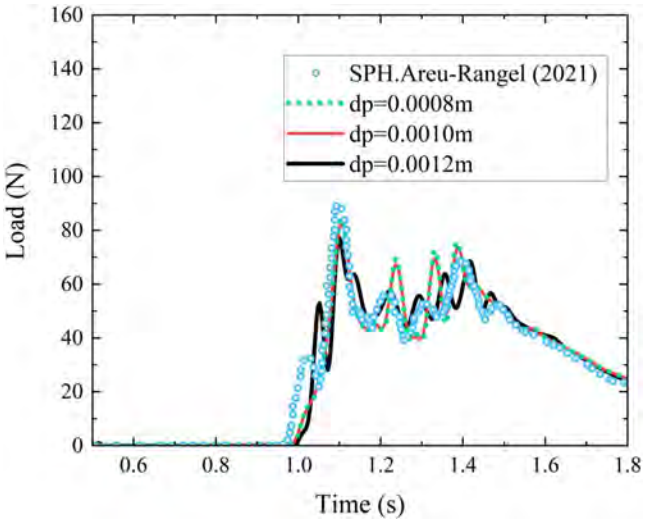

(a) Element1

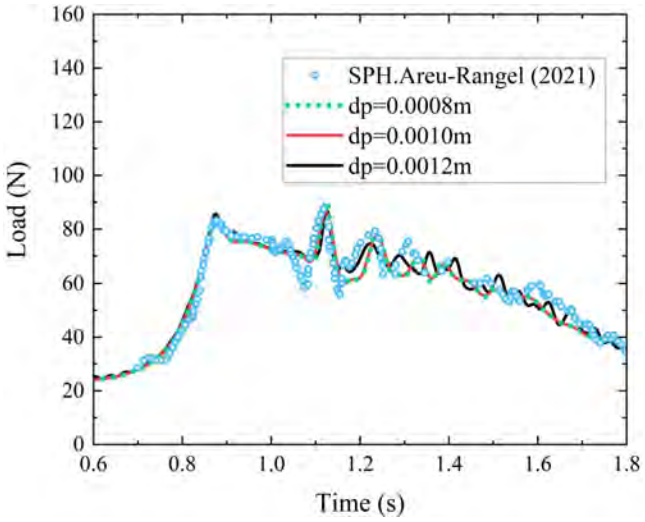

(b) Element2

Fig. 5 Validation of the numerical approach: Comparison of the loads of elements between the SPH results and MPS results with three different particle spacings: (a) Vertical loads of Element1 and (b) horizontal loads of Element2

Convergence studies were also performed for verification. Convergence studies were carried out on particle spacing (dp) with three particle resolutions in terms of 0.0008 m, 0.001 m, and 0.0012 m. Figure 3 shows a summary of these tests. The convergence of wave elevations and loads of element to particle spacing was presented in Figs. 4 and 5, respectively. It can be seen that the numerical results converged as the particle spacing was decreased. The result of $dp = 0.0008$ m and $dp = 0.001$ m showed great similarity with each other. Finally, the particle spacing of 0.001 m would be used in the following studies.

Figures 4 and 5 also shows the comparison between the SPH simulation and MPS simulation. It can be seen from the water elevations measured at WP0, WP1, and WP2 in Fig. 4 that the elevations of SPH and MPS simulations when particle spacing was 0.001 m were roughly the same, which proved that there was a great similarity between the wave patterns of the MPS simulation and the SPH simulation in the left side of the tank.

Figure 5 shows the loads measured on Element1 and Element2, which indicated that the results of SPH and MPS were highly consistent in terms of trends and peak values.

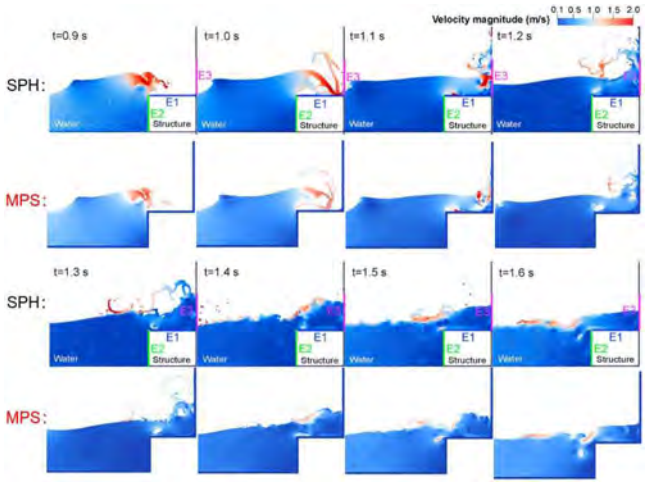

Fig. 6 Snapshots of the velocity fields of some relevant stages observed during the simulations using the SPH method (Areu-Rangel et al., 2021) and the MPS method

Figure 6 shows the velocity field comparison diagram of SPH simulation and the simulation of the MLParticle-SJTU solver used in this paper. It can be seen that the wave patterns and velocity fields of these two simulations were quite similar. After the incident wave reached the left edge of the structure, it broke, and then the incident wave hit the upper deck of the structure and travelled across the deck to the left and right. Some of the incident waves also hit the junction of the superstructure and the deck. With more and more water on the deck, the water began to climb up along the superstructure wall, fell back, and flowed down from the deck. In the phase where the wave struck the deck and propagated to the left side on the deck, a cavity appeared near the left edge of the deck.

In summary, the numerical simulation results using the MPS method shown in this paper had a high similarity with the results of Areu-Rangel et al., which verified the accuracy of the numerical simulation method used in this paper. This simulation model can be used for the next numerical simulations.

Effect of the Gate Release Velocity in Wave Pattern and Loads

To study the influence of the gate release on the wave formation and the green water events generated, four different gate release speeds were used to generate incident waves: 1 m/s, 1.6 m/s, 2 m/s, and 5 m/s. Only the gate release velocity of 1 m/s did not ensure an open time $t < (2h/g)^{0.5}$, where g is gravitational acceleration and h is the initial water level upstream of the gate. The thickness of the gate was 0.01 m, which was the same as in the experimental setting of Hernández-Fontes et al. (2020). The gate was driven by a free-fall weight mounted in the experiment, and more details of the instrumentation involved in the experiment can be found in Hernández-Fontes et al. (2018).

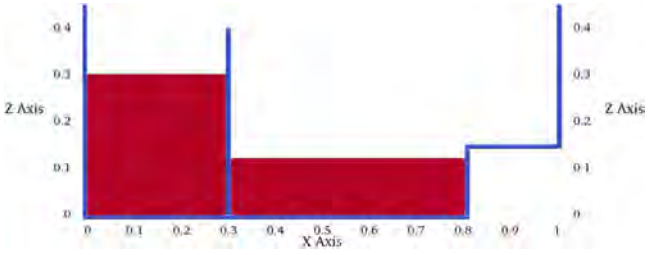

Fig. 7 The sketch of the model used in MPS simulation

The numerical simulation model and settings used are shown in Fig. 7, which is consistent with the model of the above verification procedure, except for a gate with a width of 0.01 m. The settings of three wave probes and two elements were the same as those shown in Fig. 1. The initial particle spacing was set to 0.001 m.

Hernández-Fontes et al. (2020) showed the results of the wet dam-break experiment of the same model as this paper, but they did not provide information about the gate release speed. The results of this experiment were also compared with the results of the MPS simulation.

Figures 8∼13 show representative snapshots of the experiments of Hernández-Fontes et al. (2020) and MPS simulations at different gate release speeds. It can be seen that when the gate release speed was 1.6 m/s, the wave patterns of numerical simulation were almost in agreement with the experimental data. When the gate speed was less than 2 m/s, the incident wave at 0.97 s was relatively complete. Broken bores can be observed in the cases of higher speeds. An incident wave with multiple jets occurred at a gate velocity of 5 m/s.

Figures 14∼16 show that different gate release speeds produced different incident waves of green water events. The water body on the left side of the gate at the initial time is referred to as W1, and the water body on the right side of the gate at the initial time is referred to as W2 in the following discussion. In the case of low

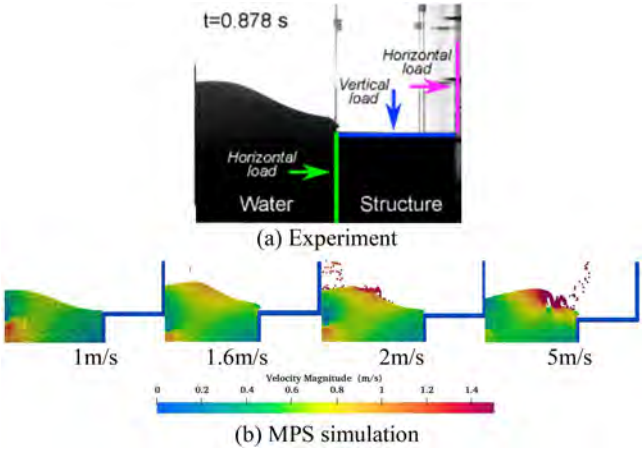

Fig. 8 Snapshots found in the experiment of Hernández-Fontes et al. (2020) and MPS simulations with different gate speeds at 0.878 s

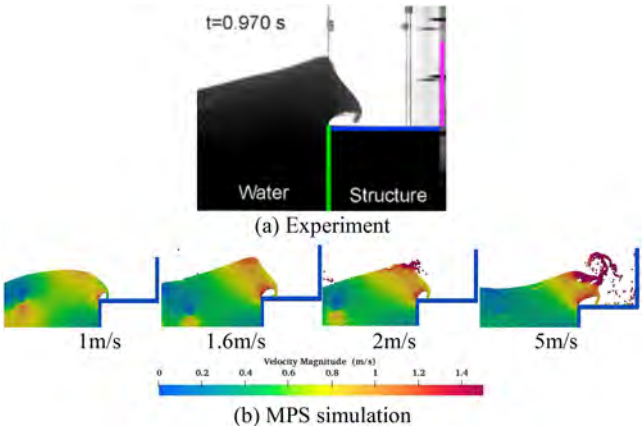

Fig. 9 Snapshots found in the experiment of Hernández-Fontes et al. (2020) and MPS simulations with different gate speeds at 0.970 s

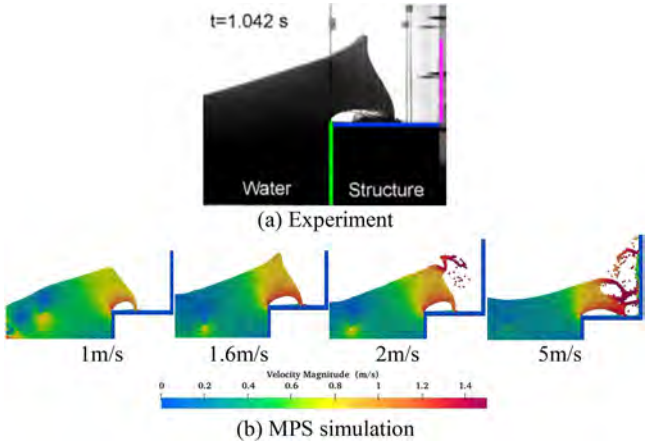

Fig. 10 Snapshots found in the experiment of Hernández-Fontes et al. (2020) and MPS simulations with different gate speeds at 1.042 s

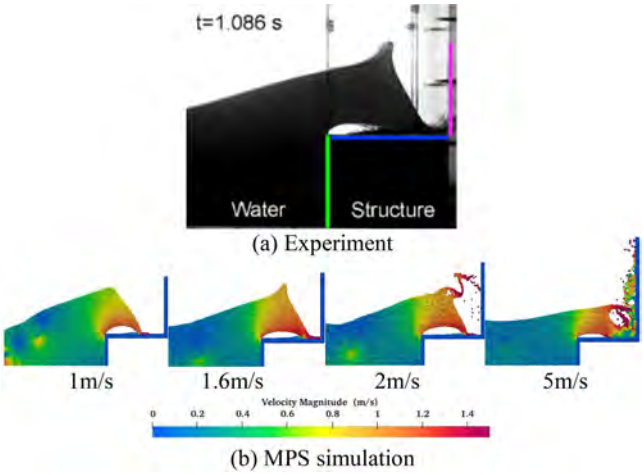

Fig. 11 Snapshots found in the experiment of Hernández-Fontes et al. (2020) and MPS simulations with different gate speeds at 1.086 s

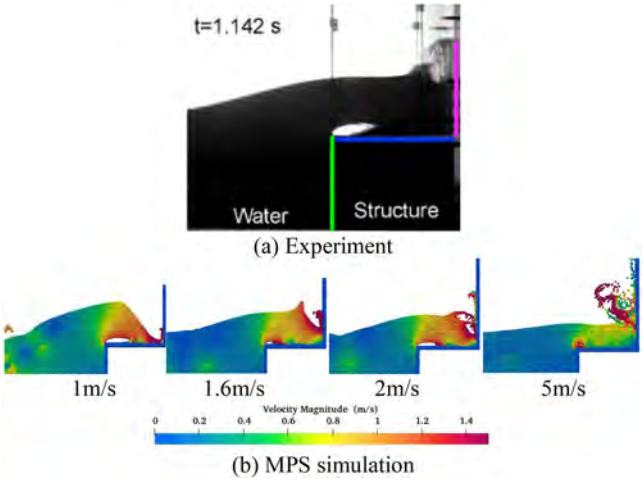

Fig. 12 Snapshots found in the experiment of Hernández-Fontes et al. (2020) and MPS simulations with different gate speeds at 1.142 s

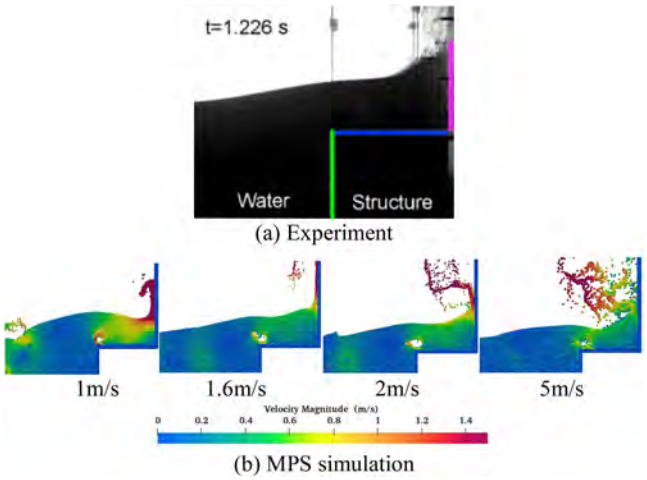

Fig. 13 Snapshots found in the experiment of Hernández-Fontes et al. (2020) and MPS simulations with different gate speeds at 1.226 s

gate speed, as shown in Fig. 14, W1 flowed from the gap under the gate into the lower part of W2. W2 was then jacked up by W1, and W1 continued to spread to the right, as shown in Fig. 15. The rightward propagating W1 subsequently reached the vicinity of the left side of the structure and squeezed W2 near the structure.

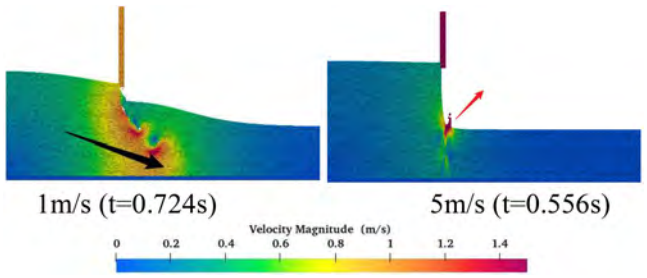

Fig. 14 Snapshots of the moments contact of gate and water ends

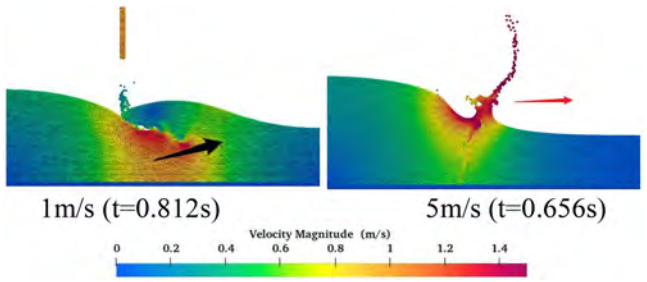

Fig. 15 Snapshots of the different wave patterns generated by different gate speeds

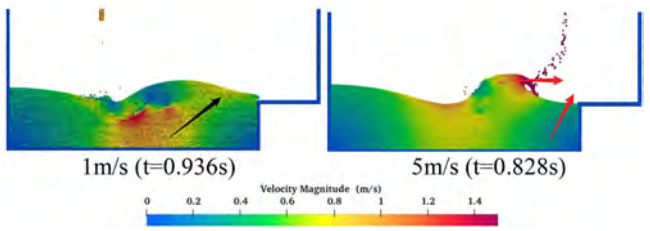

Fig. 16 Snapshots of the different incident waves of green water events generated by different gate speeds

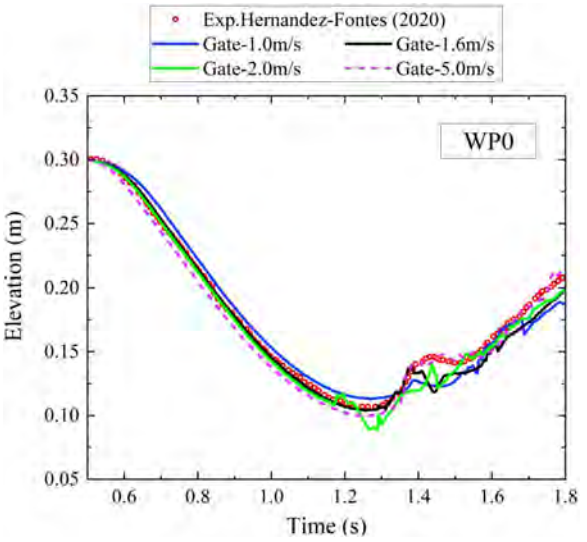

(a) WP0

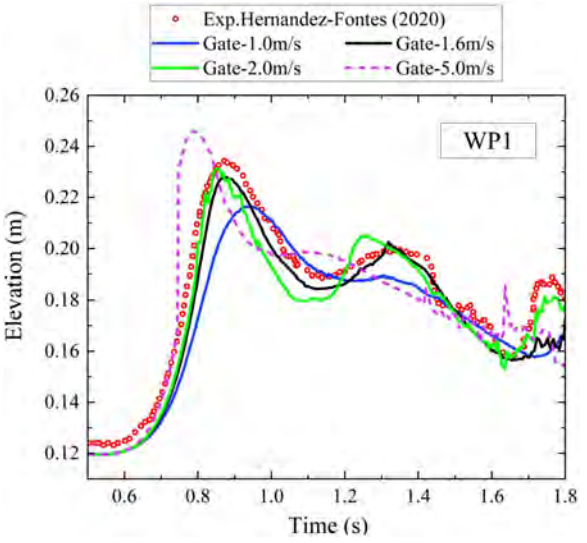

(b) WP1

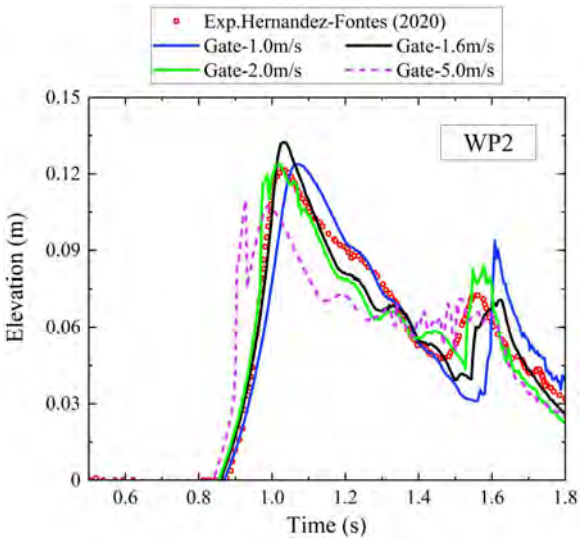

(c) WP2

Fig. 17 Wave elevations at different gate release speeds and wave elevations of the experiment (Hernández-Fontes et al., 2020): (a) Water elevations at WP0, (b) water elevations at WP1, and (c) water elevations at WP2

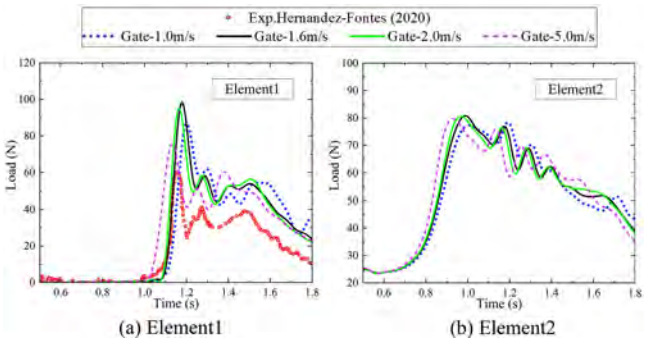

Fig. 18 Loads of elements at different gate release speeds and loads of elements of the experiment (Hernández-Fontes et al., 2020): (a) Vertical loads of Element1 and (b) horizontal loads of Element2

As a result of the interaction between W1 and W2, part of W2 climbed up along the left wall of the structure, and W1 moved toward the upper right side and lifted W2 up, forming the incident wave of green water event, as shown in Fig. 16. With high gate release speed, the interaction time between the gate and the water was short, and the water did not deform much when the gate left W1, as shown in Fig. 14. After the gate left W1, the two bodies of water of different heights squeezed each other to form a wave at the middle junction. This wave on the free surface propagated to the right. When it reached the structure, it encountered the water coming up from the left side of the structure, as shown in Fig. 16 and Figs. 8 and 9, resulting in the broken incident wave of green water events. With the gate speed of 5 m/s, the flow field was close to the flow field generated by the ideal wet dam-break method without a gate. It can also be seen that in the case of low gate speed, the water body with high kinetic energy was below the water surface, and in the case of high gate speed, the water body with high kinetic energy was on the free surface. In summary, the way in which the incident waves of the green water events were generated was different with different gate release speeds. The way of generating the incident wave with medium gate speeds (1.6 m/s and 2 m/s) can be seen as a combination of that with speeds of 1 m/s and 5 m/s.

It can be seen from the elevation curves at WP0 in Fig. 17 that the slower the gate speed, the slower the left water body dropped. This was due to the blocking effect of the gate on the left water body. From the elevation curves at WP1 (Fig. 17), it can be seen that as the gate speed increased, the peak value of elevation at WP1 increased, and the peak value of the elevation arrived earlier. The gate release speeds were different, the way the incident waves were generated was different, and the speeds of wave propagation were also different. The greater the gate release velocity, the greater the mutual squeezing action between W1 and W2 at the intermediate junction, and the greater the height of the wave formed on the free surface. Similar to WP0 and WP1, the higher the gate speed, the earlier the peak value of WP2 was reached. However, the peak of WP2 with a gate speed of 1.6 m/s was maximum. When the gate release velocity was too low, the incident waves on the deck were essentially generated by W1 lifting W2. It can be seen from Figs. 9∼11 that there was an upward jet at the crest of the incident wave with a gate release speed of 1.6 m/s compared with that with a gate speed of 1 m/s, and this jet resulted in a smaller value of the peak of the elevation with a gate speed of 1 m/s compared with that with a speed of 1.6 m/s. This wave jet was formed by the rightward moving wave on the free surface. In the case of the largest gate release speed, an incident wave of a green water event was formed by the rightward

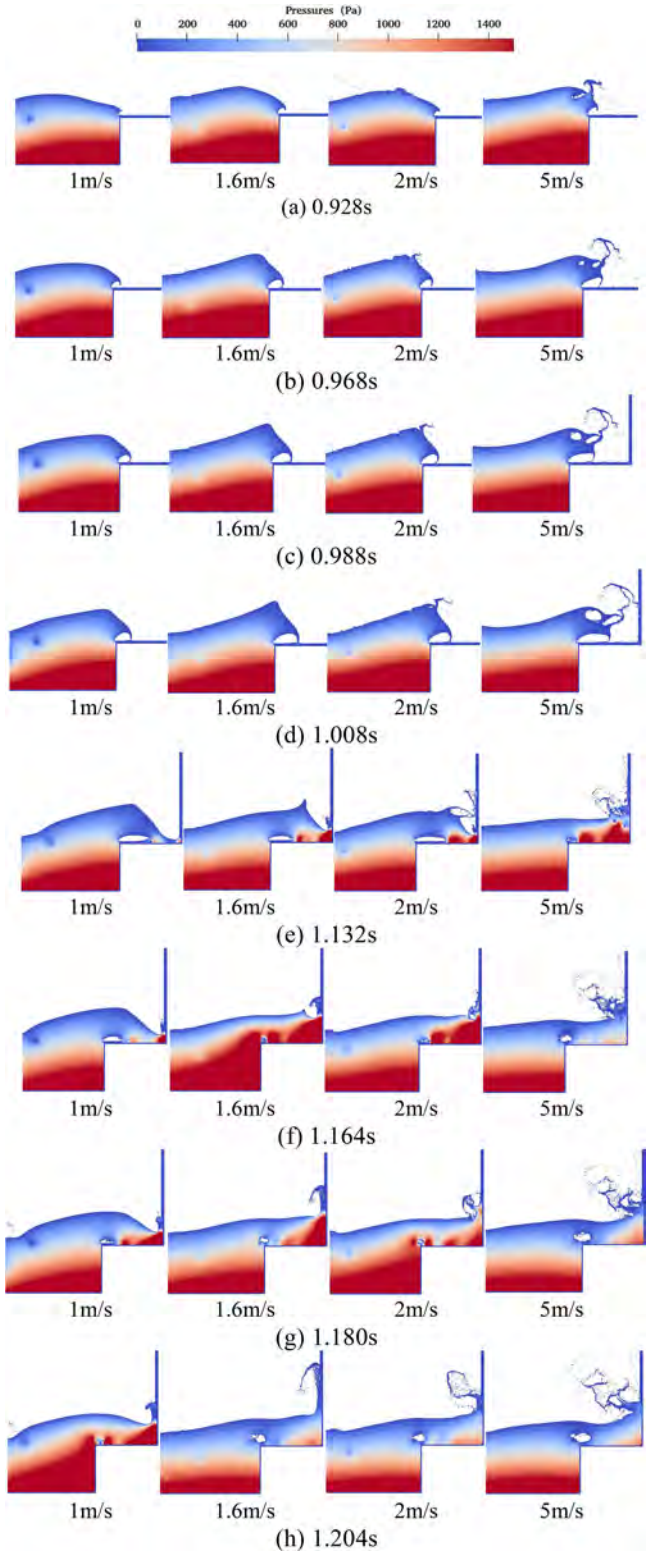

Fig. 19 Snapshots of pressure fields found in MPS simulations with different gate speeds at different times

moving wave on the free surface and the water climbing up near structure, which lacked the lifting effect of W1 in the case of small gate velocities, resulting in a decrease in the peak elevation value.

In addition, the experimental results of Hernández-Fontes et al. (2020) are compared with the MPS numerical simulation results

in Fig. 17, which verifies the accuracy of wave patterns in the numerical simulation to some extent.

From the vertical load of Element1 (Fig. 18), it can be seen that the higher the gate release speed, the earlier the peak of the load was reached, which was similar to the trend of the elevation curve of WP2. The maximum vertical loads occurred when the incident wave hit the upper deck in a large area. The peak value of the vertical load of Element1 at the gate speed of 1.6 m/s was the largest. The low gate speed would contribute to an incoming wave hitting the deck more gently, resulting in a reduction of the peak load value. If the gate speed was too high, waves would collide and break near the left wall of the structure, and some of the water would be hindered and flow back into the tank, reducing the water volume of the green water event and the peak value of load. The effect of the gate release speed on the peak value of the horizontal load on Element2 was similar to that on the peak value of wave elevation at WP2. In addition to hydrostatic pressure, the kinetic energy of the water near the left side of the structure also influenced the horizontal load of Element2. Therefore, the relationships of the peak loads of Element2 and the wave elevations at the WP2 measuring point were slightly different.

Furthermore, the load on the structure in the Hernández-Fontes et al. experiment was much lower than that in the MPS simulation when the gate speed was 1.6 m/s, which may be due to the cavity generated at the left edge of the structure deck. The numerical simulation in this paper did not consider the air phase, which would have a certain impact on the results. In addition, the numerical simulation was two-dimensional, whereas the experiment was three-dimensional, which may also have an effect on the experimental results. Nevertheless, the trend of the experimental load was very similar to the numerical simulation result of the gate speed of 1.6 m/s, indicating that the analysis in this paper was still effective.

Figure 19 shows snapshots of the pressure fields at the moments of peak loads. Significant pressures occurred at the connection between the superstructure and the deck of the structure, which was detrimental to the structure.

CONCLUSIONS

In this paper, the solver MLParticle-SJTU based on the MPS method was used to simulate and analyze the influence of different gate release speeds on the incident wave patterns generated by the wet dam-break method and the loads of the fixed structure under the given model parameters. Several conclusions can be drawn from the analysis of the results. First, the simulations with different gate release speeds generated incident waves in different ways, and the wave patterns were different. The higher the speed, the more likely the incident wave was broken before boarding the deck. Second, the higher the release speed of the gate, the earlier the wave loads of the structure reached the peak. Third, the peak values of the wave loads reached the maximum at a certain release speed. As the release speed of the gate increased or decreased, the peak values of the wave loads decreased. The results of this paper can provide a reference for subsequent experiments or numerical simulations based on the wet dam-break method. Further research is recommended to include multiphases in the modelling and to study freely moving or deformable structures.

ACKNOWLEDGEMENTS

This work was supported by the National Natural Science Foundation of China (Grant 52131102), to which the authors are most grateful.

REFERENCES

Areu-Rangel, OS, Hernández-Fontes, JV, Silva, R, Esperanca, PTT, and Klapp, J (2021). "Green Water Loads Using the Wet Dam-break Method and SPH," *Ocean Eng*, 219, 108392. https://doi.org/10.1016/j.oceaneng.2020.108392.

Ataie-Ashtiani, B, and Farhadi, L (2006). "A Stable Moving-particle Semi-implicit Method for Free Surface Flows," *Fluid Dyn Res*, 38(4), 241–256. https://doi.org/10.1016/j.fluiddyn.2005.12.002.

Chen, X, and Wan, D (2019). "GPU Accelerated MPS Method for Large-scale 3-D Violent Free Surface Flows," *Ocean Eng*, 171, 677–694. https://doi.org/10.1016/j.oceaneng.2018.11.009.

Fonseca, N, and Soares, CG (2005). "Experimental Investigation of the Shipping of Water on the Bow of a Containership," *J Offshore Mech Arct Eng*, 127(4), 322–330. https://doi.org/10.1115/1.2087527.

Garoosi, F, Mellado-Cusicahua, AN, Shademani, M, and Shakibaeinia, A (2022). "Experimental and Numerical Investigations of Dam Break Flow over Dry and Wet Beds," *Int J Mech Sci*, 215, 106946. https://doi.org/10.1016/j.ijmecsci.2021.106946.

Greco, M, Colicchio, G, and Faltinsen, OM (2007). "Shipping of Water on a Two-dimensional Structure. Part 2," *J Fluid Mech*, 581, 371–399. https://doi.org/10.1017/S002211200700568X.

Greco, M, Landrini, M, and Faltinsen, OM (2004). "Impact Flows and Loads on Ship-deck Structures," *J Fluids Struct*, 19(3), 251–275. https://doi.org/10.1016/j.jfluidstructs.2003.12.009.

Hernández-Fontes, JV, Vitola, MA, Esperanca, PTT, Sphaier, SH, and Silva, R (2020). "Patterns and Vertical Loads in Water Shipping in Systematic Wet Dam-break Experiments," *Ocean Eng*, 197, 106891. https://doi.org/10.1016/j.oceaneng.2019.106891.

Hernández-Fontes, JV, Vitola, MA, Silva, MC, Esperança, PDTT, and Sphaier, SH (2018). "On the Generation of Isolated Green Water Events Using Wet Dam-break," *J Offshore Mech Arct Eng*, 140(5), 051101.1–051101.10. https://doi.org/10.1115/1.4040050.

Kawamura, K, Hashimoto, H, Matsuda, A, and Terada, D (2016). "SPH Simulation of Ship Behaviour in Severe Water-shipping Situations," *Ocean Eng*, 120, 220–229. https://doi.org/10.1016/j.oceaneng.2016.04.026.

Khayyer, A, and Gotoh, H (2010). "On Particle-based Simulation of a Dam Break over a Wet Bed," *J Hydraul Res*, 48(2), 238–249. https://doi.org/10.1080/00221681003726361.

Khayyer, A, and Gotoh, H (2011). "Enhancement of Stability and Accuracy of the Moving Particle Semi-implicit Method," *J Comput Phys*, 230(8), 3093–3118. https://doi.org/10.1016/j.jcp.2011.01.009.

Khayyer, A, Gotoh, H, Falahaty, H, Shimizu, Y, and Nishijima, Y (2017). "Towards Development of a Reliable Fully-Lagrangian MPS-based FSI Solver for Simulation of 2D Hydroelastic Slamming," *Ocean Syst Eng*, 7(3), 299–318. https://doi.org/10.12989/ose.2017.7.3.299.

Khayyer, A, Shimizu, Y, Gotoh, T, and Gotoh, H (2023). "Enhanced Resolution of the Continuity Equation in Explicit Weakly Compressible SPH Simulations of Incompressible Free-surface Fluid Flows," *Appl Math Model*, 116, 84–121. https://doi.org/10.1016/j.apm.2022.10.037.

Koshizuka, S, and Oka, Y (1996). "Moving-particle Semi-implicit Method for Fragmentation of Incompressible Fluid," *Nucl Sci Eng*, 123(3), 421–434. https://doi.org/10.13182/NSE96-A24205.

Le Touzé, D, et al. (2010). "SPH Simulation of Green Water and Ship Flooding Scenarios," *J Hydrodyn*, 22(5), 231–236. https://doi.org/10.1016/S1001-6058(09)60199-2.

Luo, M, Khayyer, A, and Lin, P (2021). "Particle Methods in Ocean and Coastal Engineering," *Appl Ocean Res*, 114, 102734. https://doi.org/10.1016/j.apor.2021.102734.

Nielsen, KB, and Mayer, S (2004). "Numerical Prediction of Green Water Incidents," *Ocean Eng*, 31(3–4), 363–399. https://doi.org/10.1016/j.oceaneng.2003.06.001.

Rosetti, GF, et al. (2019). "CFD and Experimental Assessment of Green Water Events on an FPSO Hull Section in Beam Waves," *Mar Struct*, 65, 154–180. https://doi.org/10.1016/j.marstruc.2018.12.004.

Shibata, K, and Koshizuka, S (2007). "Numerical Analysis of Shipping Water Impact on a Deck Using a Particle Method," *Ocean Eng*, 34(3–4), 585–593. https://doi.org/10.1016/j.oceaneng.2005.12.012.

Shibata, K, Koshizuka, S, Sakai, M, and Tanizawa, K (2012). "Lagrangian Simulations of Ship-wave Interactions in Rough Seas," *Ocean Eng*, 42, 13–25. https://doi.org/10.1016/j.oceaneng.2012.01.016.

Shimizu, Y, Khayyer, A, Gotoh, H, and Nagashima, K (2020). "An Enhanced Multiphase ISPH-based Method for Accurate Modeling of Oil Spill," *Coastal Eng J*, 62(4), 625–646. https://doi.org/10.1080/21664250.2020.1815362.

Silva, DFC, Esperança, PTT, and Coutinho, ALGA (2017). "Green Water Loads on FPSOs Exposed to Beam and Quartering Seas, Part II: CFD Simulations," *Ocean Eng*, 140, 434–452. https://doi.org/10.1016/j.oceaneng.2016.11.008.

Tanaka, M, and Masunaga, T (2010). "Stabilization and Smoothing of Pressure in MPS Method by Quasi-compressibility," *J Comput Phys*, 229(11), 4279–4290. https://doi.org/10.1016/j.jcp.2010.02.011.

Tang, Z, Wan, D, Chen, G, and Xiao, Q (2016). "Numerical Simulation of 3D Violent Free-surface Flows by Multi-resolution MPS Method," *J Ocean Eng Mar Energy*, 2(3), 355–364. https://doi.org/10.1007/s40722-016-0062-6.

Tang, Z, Zhang, Y, and Wan, D (2016). "Multi-resolution MPS Method for Free Surface Flows," *Int J Comput Methods*, 13(4), 1641018. https://doi.org/10.1142/S0219876216410188.

von Häfen, H, Goseberg, N, Stolle, J, and Nistor, I (2019). "Gate-opening Criteria for Generating Dam-break Waves," *J Hydraul Eng*, 145(3), 04019002. https://doi.org/10.1061/(ASCE)HY.1943-7900.0001567.

Wen, X, Zhao, W, and Wan, D (2021a). "A Multiphase MPS Method for Bubbly Flows with Complex Interfaces," *Ocean Eng*, 238, 109743. https://doi.org/10.1016/j.oceaneng.2021.109743.

Wen, X, Zhao, W, and Wan, D (2021b). "An Improved Moving Particle Semi-implicit Method for Interfacial Flows," *Appl Ocean Res*, 117, 102963. https://doi.org/10.1016/j.apor.2021.102963.

Ye, Z, and Zhao, X (2017). "Investigation of Water-water Interface in Dam Break Flow with a Wet Bed," *J Hydrol*, 548, 104–120. https://doi.org/10.1016/j.jhydrol.2017.02.055.

Zhang, G, Chen, X, and Wan, D (2019). "MPS-FEM Coupled Method for Study of Wave-structure Interaction," *J Mar Sci Appl*, 18(4), 387–399. https://doi.org/10.1007/s11804-019-00105-6.

Zhang, S, Yue, DK-P, and Tanizawa, K (1996). "Simulation of Plunging Wave Impact on a Vertical Wall," *J Fluid Mech*, 327, 221–254. https://doi.org/10.1017/S002211209600852X.

Zhang, Y, Tang, Z, and Wan, D (2016). "Simulation of Solitary Wave Interacting with Flat Plate by MPS Method," *Chin J Hydrodyn*, 31(4), 395–401. https://doi.org/10.16076/j.cnki.cjhd.2016.04.001.

Zhang, Y, Wan, D, and Hino, T (2014). "Application of MPS Method in Liquid Sloshing," *Ocean Eng*, 32(4), 24–32. https://doi.org/10.16483/j.issn.1005-9865.2014.04.002.

Zhang, ZL, Khalid, MSU, Long, T, Liu, MB, and Shu, C (2021). "Improved Element-particle Coupling Strategy with δ-SPH and Particle Shifting for Modeling Sloshing with Rigid or Deformable Structures," *Appl Ocean Res*, 114, 102774. https://doi.org/10.1016/j.apor.2021.102774.